

# Formation of deeply bound ultracold Sr<sub>2</sub> molecules by photoassociation near the <sup>1</sup>S + <sup>3</sup>P<sub>1</sub> intercombination line

Wojciech Skomorowski and Robert Moszynski

*Quantum Chemistry Laboratory, Department of Chemistry, University of Warsaw, Pasteura 1, 02-093 Warsaw, Poland*

Christiane P. Koch\*

*Theoretische Physik, Universität Kassel, Heinrich-Plett-Straße 40, 34132 Kassel, Germany*

(Received 20 March 2012; published 17 April 2012)

We predict feasibility of the photoassociative formation of Sr<sub>2</sub> molecules in arbitrary vibrational levels of the electronic ground state based on state-of-the-art *ab initio* calculations. Key is the strong spin-orbit interaction between the  $c^3\Pi_u$ ,  $A^1\Sigma_u^+$ , and  $B^1\Sigma_u^+$  states. It creates not only an effective dipole moment allowing free-to-bound transitions near the <sup>1</sup>S + <sup>3</sup>P<sub>1</sub> intercombination line but also facilitates bound-to-bound transitions via resonantly coupled excited-state levels to deeply bound levels of the ground  $X^1\Sigma_g^+$  potential, with  $v''$  as low as  $v'' = 6$ . The spin-orbit interaction is responsible for both optical pathways. Therefore, those excited-state levels that have the largest bound-to-bound transition moments to deeply bound ground-state levels also exhibit a sufficient photoassociation probability, comparable to that of the lowest weakly bound excited-state level previously observed by Zelevinsky *et al.* [*Phys. Rev. Lett.* **96**, 203201 (2006)]. Our study paves the way for an efficient photoassociative production of Sr<sub>2</sub> molecules in ground-state levels suitable for experiments testing the electron-to-proton mass ratio.

DOI: 10.1103/PhysRevA.85.043414

PACS number(s): 34.80.Qb, 33.80.-b, 33.70.-w

## I. INTRODUCTION

The cooling and trapping of alkaline-earth metals and systems with a similar electronic structure have attracted significant attention over the last decade. The interest in ultracold gases of alkaline-earth-metal atoms was triggered by the quest for new optical frequency standards [1]. The extremely narrow linewidth of the intercombination <sup>1</sup>S + <sup>3</sup>P<sub>1</sub> transition, together with the magic wavelength of an optical lattice [2], is at the heart of the clock proposals. Strontium is the atomic species of choice in many current clock experiments [3–6]. The narrow width of the intercombination line implies Doppler temperatures as low as 0.5 μK for laser cooling [7]. It also allows for easy optical control of the atom-atom interactions via optical Feshbach resonances that involve only small losses [8,9].

The diatomic strontium molecule represents a candidate for high-precision spectroscopy that aims at determining the time variation of the electron-to-proton mass ratio [10]. The idea is to prepare tightly confined Sr<sub>2</sub> molecules in their electronic ground state by photoassociation in an optical lattice and carry out high-precision Raman spectroscopy on the ground-state vibrational level spacings [10,11]. Photoassociation refers to the excitation of colliding atom pairs into bound levels of an electronically excited state [12]. Molecules in their electronic ground state are obtained by spontaneous decay [13]. Whether the excited-state molecules redissociate or decay into bound ground-state levels is determined by the shape of the excited-state potential curve and possibly its coupling to other excited states. Long-range potential wells and strong spin-orbit interaction in the excited state of alkali-metal dimers were

found to yield significant bound-to-bound transition matrix elements [14].

To date, Sr<sub>2</sub> molecules in their excited state have been formed by photoassociation, using both a dipole-allowed transition [15,16] and a dipole-forbidden transition near the <sup>1</sup>S + <sup>3</sup>P<sub>1</sub> intercombination line [17,18]. The formation of Sr<sub>2</sub> molecules in their electronic ground state has not yet been demonstrated except for the very last bound level [18]. After photoassociation using the dipole-allowed transition, the majority of the excited-state molecules redissociates, and only the last two bound levels of the electronic ground state can be populated [19]. This is due to the long-range  $R^{-3}$  nature of the electronically excited state (with  $R$  denoting the interatomic separation) that does not provide any mechanism for efficient stabilization to bound ground-state levels [20]. The situation changes for photoassociation near the intercombination line where the excited-state potential curve in the asymptotic region behaves predominantly as  $R^{-6}$  with a small  $\delta C_3^{\text{res}} R^{-3}$  correction, where  $\delta C_3^{\text{res}}$  is proportional to  $\alpha^4$  (with  $\alpha$  the fine-structure constant). Large bound-to-bound transition matrix elements with the electronic ground state that behaves asymptotically as  $R^{-6}$  are then expected [17]. However, quantitative estimates on which ground-state levels can be accessed were hampered to date due to lack of reliable *ab initio* information on the excited-state potential-energy curves and, importantly, the spin-orbit interaction. The latter is crucial because it yields the effective dipole moment that is utilized in the photoassociation transition and also governs possible bound-to-bound transitions following the photoassociation.

Here, we consider the photoassociation process of two ultracold strontium atoms into the manifold of the coupled  $c^3\Pi_u(^1S + ^3P) + A^1\Sigma_u^+(^1S + ^1D) + B^1\Sigma_u^+(^1S + ^1P)$  states. The excited-state potential-energy curves, spin-orbit coupling, and transition dipole matrix elements are obtained by state-of-the-art *ab initio* calculations [21]. This allows us to

\*christiane.koch@uni-kassel.de

make quantitative predictions on the photoassociation rates, bound-to-bound transition matrix elements, and spontaneous emission coefficients. We find that the spin-orbit interaction alters parts of the excited-state vibrational spectrum qualitatively, opening the way for transitions into deeply bound ground-state levels. This implies that the standard picture of pure Franck-Condon-type transitions near the classical turning points in the ground- and a single excited-state potential-energy curve yields qualitatively wrong predictions. The crossing between the  $c^3\Pi_u(^1S + ^3P)$  and  $A^1\Sigma_u^+(^1S + ^1D)$  states is found to also significantly affect the transition moments for the Raman spectroscopy envisioned for the test of the electron-to-proton mass ratio. The paper is organized as follows: Sec. II introduces our model and briefly reviews the theoretical methods employed. The numerical results are presented in Sec. III, and Sec. IV concludes our paper.

## II. THEORY

When a pair of colliding atoms absorbs a photon, it undergoes a transition from the scattering continuum of the  $X^1\Sigma_g^+$  ground electronic state into a bound rovibrational level of an electronically excited state. Here, we consider photoassociation using a continuous-wave laser that is red detuned with respect to the  $^3P_1$  intercombination line of strontium. This transition is dipole forbidden in the non-relativistic approximation. The  $c^3\Pi$  state, correlating to the

asymptote of the intercombination line transition, is, however, coupled by the spin-orbit interaction to two singlet states,  $A^1\Sigma_u^+$  and  $B^1\Sigma_u^+$ . Both singlet states are connected by a dipole-allowed transition to the ground electronic state  $X^1\Sigma_g^+$ . Thus an effective transition matrix element is created which for moderate and large interatomic separations is well approximated by

$$d_{SO} = \frac{\langle X^1\Sigma_g^+ | \hat{d}_z | B^1\Sigma_u^+ \rangle \langle B^1\Sigma_u^+ | \hat{H}_{SO} | c^3\Pi_u \rangle}{E_{c^3\Pi_u} - E_{B^1\Sigma_u^+}} + \frac{\langle X^1\Sigma_g^+ | \hat{d}_z | A^1\Sigma_u^+ \rangle \langle A^1\Sigma_u^+ | \hat{H}_{SO} | c^3\Pi_u \rangle}{E_{c^3\Pi_u} - E_{A^1\Sigma_u^+}}, \quad (1)$$

where  $\hat{H}_{SO}$  is the spin-orbit Hamiltonian in the Breit-Pauli approximation [22]. The long-range part of  $d_{SO}$ , dominated by the first term in the above expression, is due to the coupling with the  $B^1\Sigma_u^+$  state, ideally suited for photoassociation. The short-range part is due to the coupling with the  $A^1\Sigma_u^+$  state, paving the way toward efficient stabilization of the photoassociated molecules to the electronic ground state, as we will show below. The scheme for photoassociation into the lowest manifold of Hund's case (c)  $0_u^+$  states is depicted in Fig. 1.

We will make use of nonadiabatic effects caused by the spin-orbit interaction and therefore employ the diabatic [Hund's case (a)] picture for our calculations. The corresponding Hamiltonian in the rotating-wave approximation reads

$$\hat{\mathbb{H}} = \begin{pmatrix} \hat{H}_{\text{diag}}^{X^1\Sigma_g^+} & 0 & \frac{1}{2}d_z(A \leftarrow X)E_0 & \frac{1}{2}d_z(B \leftarrow X)E_0 \\ 0 & \hat{H}_{\text{diag}}^{c^3\Pi_u^+} - A(R) - \Delta_{\omega_1} & \xi_1(R) & \xi_2(R) \\ \frac{1}{2}d_z(A \leftarrow X)E_0 & \xi_1(R) & \hat{H}_{\text{diag}}^{A^1\Sigma_u^+} - \Delta_{\omega_1} & 0 \\ \frac{1}{2}d_z(B \leftarrow X)E_0 & \xi_2(R) & 0 & \hat{H}_{\text{diag}}^{B^1\Sigma_u^+} - \Delta_{\omega_1} \end{pmatrix} \quad (2)$$

where  $d_z(n \leftarrow X)$  denotes the  $z$  component of the electronic transition dipole moment from the  $X$  electronic ground state to an electronically excited state  $n$ .  $R$  is the interatomic separation. The peak amplitude and the detuning of the photoassociation laser with respect to the intercombination line are represented by  $E_0$  and  $\Delta_{\omega_1}$ , respectively. The diagonal terms for the  $(n)^{(2S+1)}|\Lambda\rangle$  state are given by

$$\hat{H}_{\text{diag}}^{(n)^{(2S+1)}|\Lambda\rangle} \equiv \frac{1}{2\mu} \frac{\partial^2}{\partial R^2} + V_n^{(2S+1)|\Lambda}(R) + \frac{J(J+1) + S(S+1) - \Omega^2 - \Sigma^2 + L(L+1) - \Lambda^2}{2\mu R^2}, \quad (3)$$

with  $\mu$  denoting the reduced mass,  $V_n^{(2S+1)|\Lambda}(R)$  the radial potential energy curve,  $J$  the rotational quantum number, and  $S$  the electronic spin quantum number.  $\Lambda$ ,  $\Sigma$ , and  $\Omega$  denote the projections of the electronic orbital angular momentum, electronic spin angular momentum, and the total angular momentum on the molecular axis, respectively. The term involving the electronic orbital quantum number  $L$  in Eq. (3) is an approximation to the true diagonal adiabatic correction [23], with  $L$  corresponding to the orbital quantum number in the separated-atom limit, cf. the discussion following Eq. (40) in Ref. [23]. The spin-orbit matrix elements are defined by

$$A(R) = \langle c^3\Pi_u(\Sigma = \pm 1, \Lambda = \mp 1) | \hat{H}_{SO} | c^3\Pi_u(\Sigma = \pm 1, \Lambda = \mp 1) \rangle \quad (4)$$

and

$$\xi_1(R) = \langle c^3\Pi_u(\Sigma = \pm 1, \Lambda = \mp 1) | \hat{H}_{SO} | A^1\Sigma_u^+ \rangle, \quad (5)$$

$$\xi_2(R) = \langle c^3\Pi_u(\Sigma = \pm 1, \Lambda = \mp 1) | \hat{H}_{SO} | B^1\Sigma_u^+ \rangle. \quad (6)$$

The potential energy curve for the  $X^1\Sigma_g^+$  ground electronic state was taken from Ref. [24]. All other potential energy curves, spin-orbit coupling matrix elements (shown in the left panel of Fig. 2), and electronic transition dipole moments  $d_z(n \leftarrow X)$  (shown in the right panel of Fig. 2), were obtained from state-of-the-art *ab initio* electronic structure calculations. The details of these calculations as well as their agreement with the most recent experimental data [25], in particular, for the crucial  $A^1\Sigma_u^+$  state, are reported elsewhere [21].

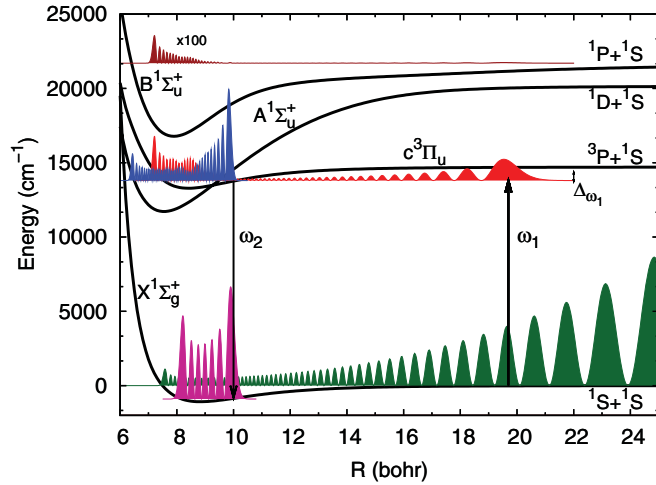


FIG. 1. (Color online) Proposed scheme for the production of ultracold Sr<sub>2</sub> molecules by photoassociation near the intercombination line. The green wave function represents a scattering state of two Sr atoms and the red, blue, and brown wave functions represent the diabatic components of the excited-state vibrational level with binding energy  $E_{v''=15} = 12.9$  cm<sup>-1</sup>. Spin-orbit interaction facilitates a transition from this level to  $X^1\Sigma_g^+ v'' = 6$  (with the corresponding wave function depicted in purple) via spontaneous or stimulated emission.

The most promising route to form Sr<sub>2</sub> molecules in their electronic ground state via photoassociation and subsequent spontaneous emission is determined by diagonalization of the full Hamiltonian (2) and analysis of its rovibrational structure. In order to connect our model to experimental observables, we calculate the photoassociation rate,  $K(\omega_1, T)$ , and the branching ratios for spontaneous emission,  $P(v'' \leftarrow v')$ . The absorption coefficient  $K(\omega_1, T)$  at laser frequency  $\omega_1$  is given by [26,27]

$$K(\omega_1, T) = \frac{2\pi\rho^2}{\hbar Q_T} \sum_{v', J'} \sum_{J''} g_{J''} (2J'' + 1) \times \int_0^\infty e^{-E/k_B T} |\mathcal{S}_{v' J'}(E, J'', \omega_1)|^2 dE, \quad (7)$$

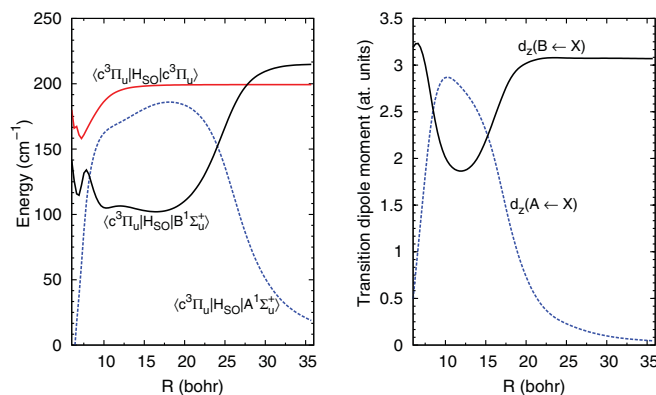


FIG. 2. (Color online) Spin-orbit couplings (left) and transition dipole moments (right) between the relevant electronic states of the Sr<sub>2</sub> dimer that enter the Hamiltonian (2).

where  $\rho$  denotes the gas number density,  $T$  the temperature,  $k_B$  the Boltzmann constant,  $v'$  and  $J'$  the vibrational and rotational quantum numbers in the electronically excited state,  $J''$  the rotational quantum number of the initial scattering state,  $g_{J''}$  the spin statistical weight depending on the nuclear spin, equal to one for <sup>88</sup>Sr, and  $Q_T = (\mu k_B T / 2\pi \hbar^2)^{3/2}$ .  $\mathcal{S}_{v' J'}(E, J'', \omega_1)$  is the  $\mathcal{S}$ -matrix element for the transition from a continuum state with scattering energy  $E$  and rotational quantum number  $J''$  into the bound level  $|v', J'\rangle$ . Throughout this paper, the quantum numbers  $J''$  and  $v''$  denote the rovibrational levels of the ground electronic state, while  $J', v'$  refer to the rovibrational levels of the excited electronic state. The square of the  $\mathcal{S}$ -matrix element in Eq. (7) can be approximated by the resonant scattering expression for an isolated resonance [26],

$$|\mathcal{S}_{v' J'}(E, J'', \omega_1)|^2 = \frac{\gamma_{v' J'}^s(E, J'') \gamma_{v' J'}^d}{[E - \Delta_{v' J'}(\omega_1)]^2 + \frac{1}{4} [\gamma_{v' J'}^s(E, J'') + \gamma_{v' J'}^d]^2}, \quad (8)$$

where  $\gamma_{v' J'}^s(E, J'')$  is the stimulated emission rate and  $\gamma_{v' J'}^d(E, J'')$  is the rate of the spontaneous decay, both in units of  $\hbar$ , and  $\Delta_{v' J'}(\omega_1)$  is the detuning relative to the position of the bound rovibrational level  $|v', J'\rangle$ , i.e.,  $\Delta_{v' J'} = E_{v' J'} - \hbar\omega_1$ , where  $E_{v' J'}$  is the binding energy of the level  $|v', J'\rangle$ . In Eq. (8), we assume the decay rate due to any other undetected processes to be negligible.

The spontaneous emission rates  $\gamma_{v' J'}^d$  are obtained from the Einstein coefficients  $A_{v' J', v'' J''}$ ,

$$\gamma_{v' J'}^d = \sum_{v'' J''} A_{v' J', v'' J''}, \quad (9)$$

and related to the natural lifetimes  $\tau_{v' J'} = \hbar / \gamma_{v' J'}^d$ . The Einstein coefficient  $A_{v' J', v'' J''}$  is given by

$$A_{v' J', v'' J''} = \frac{4\alpha^3}{3e^4 \hbar^2} H_{J'} (E_{v' J'} - E_{v'' J''})^3 \times \left| \sum_{n'} \langle \chi_{v'' J''}^n | d_z(n' \leftarrow X) | \chi_{v' J'}^{n'} \rangle \right|^2, \quad (10)$$

where  $H_{J'}$  is the so-called Hönl-London factor equal to  $(J' + 1)/(2J' + 1)$  for  $J' = J'' - 1$  and  $J'/(2J' + 1)$  for  $J' = J'' + 1$ , and  $e$  denotes the electron charge. The label  $n'$  represents all considered (singlet) dissociation limits of the excited diatomic molecule; in our case these are  $^1S + ^1P$  and  $^1S + ^1D$ . The nonadiabatic rovibrational wave functions  $\chi_{v'' J''}^n(R) = \langle R | \chi_{v'' J''}^n \rangle$  are obtained as the eigenfunctions of the coupled-channel Hamiltonian, Eq. (2), in the absence of the photoassociation laser field, i.e., for  $E_0 = 0$ . In principle, in Hund's case (a), the rovibrational wave functions  $\chi_{v'' J''}^n(R)$  could also be labeled, in addition to  $n$ ,  $v$ , and  $J$ , by the quantum numbers  $p$ ,  $S$ ,  $\Sigma$ ,  $\Lambda$ , and  $\Omega$ , denoting the parity, total electronic spin, its projection on the molecular axis, the projection of the orbital electronic angular momentum, and projection of the total electronic angular momentum on the molecular axis [23]. Since here we consider bosonic <sup>88</sup>Sr atoms which are photoassociated to form molecules in the rovibrational states of the  $0_u^+$  potential, the parity is equal to one, and the projection of the total electronic angular  $\Omega'$  is zero, which in turn implies  $\Lambda' = 0$  for singlet excited states  $n'$ .

At low laser intensity  $I$ , the stimulated emission rate is given by Fermi's golden rule expression:

$$\gamma_{v'',J''}^s(E,J') = 4\pi^2 \frac{I}{c} \sum_{M''=-J''}^{J''} \sum_{M'=-J'}^{J'} |\langle \Psi_{EJ''M''} | \hat{\mathbf{d}} \cdot \vec{\epsilon} | \Psi_{v'J'M'} \rangle|^2, \quad (11)$$

where  $\vec{\epsilon}$  denotes the vector of the laser polarization,  $c$  is the speed of light, and  $\Psi_{EJ''M''}$  and  $\Psi_{v'J'M'}$  denote the total nonadiabatic (electronic and rovibrational) wave functions of the initial and final states, respectively.  $M$  is the quantum number of the projection of the total angular momentum  $J$  on the space-fixed  $Z$  axis, and  $\hat{\mathbf{d}}$  denotes the electric dipole moment operator in the space-fixed coordinate system. After introducing the Born-Huang expansion of the nonadiabatic wave functions, Eq. (11) can further be simplified to the following form [28]:

$$\gamma_{v'',J''}^s(E,J') = 4\pi^2 \frac{I}{c} (2J'+1) H_{J'} \times \left| \sum_{n'} \langle \chi_{EJ''}^X | d_z(n' \leftarrow X) | \chi_{v'J'}^{n'} \rangle \right|^2, \quad (12)$$

where  $\chi_{EJ''}^X(R)$  are energy normalized continuum wave functions of the ground electronic state with scattering energy  $E$ . Using this notation, the transition matrix elements between coupled-channel rovibrational eigenstates become

$$\langle v'',J'' | d_z | v',J' \rangle \equiv \sum_{n'} \langle \chi_{v'',J''}^X | d_z(n' \leftarrow X) | \chi_{v',J'}^{n'} \rangle. \quad (13)$$

They are almost  $J$  independent as a result of the extremely small spacings between the rotational levels of  $\text{Sr}_2$ . We may therefore assume  $\langle v'',J'' | d_z | v',J' \rangle \approx \langle v'' | d_z | v' \rangle$  (of course, the selection rule  $J'' = J' \pm 1$  holds).

Finally, the branching ratio

$$P(v'' \leftarrow v'J') = \frac{\sum_{J''} A_{v'J',v''J''}}{\sum_{v'',J''} A_{v'J',v''J''}} \quad (14)$$

describes the probability for the spontaneous decay from the level  $|v',J'\rangle$  of the electronically excited state to rovibrational levels  $|v'',J'' = J' \pm 1\rangle$  of the ground electronic state. Again, the branching ratio  $P(v'' \leftarrow v'J')$  is nearly independent of the  $J'$  quantum number.

### III. NUMERICAL RESULTS AND DISCUSSION

We consider  $^{88}\text{Sr}$  atoms trapped at a temperature of  $T \sim 2 \mu\text{K}$ , typical for the two-color magneto-optical traps employed for the alkaline-earth-metal species [29]. At such a low temperature, the collisions are purely  $s$  wave, i.e.,  $J'' = 0$ . The Hamiltonian (2) is represented on a Fourier grid with an adaptive step size [30–32].

The photoassociation yield is determined by the ground-state scattering length and the rovibrational structure of the levels in the excited  $c^3\Pi_u$ ,  $A^1\Sigma_u^+$ , and  $B^1\Sigma_u^+$ -state manifolds which couple to  $0_u^+$  symmetry. The correct ground-state scattering properties including the scattering length are accounted for by employing the empirical  $X^1\Sigma_g^+$  potential reported in Ref. [24], reflecting the current spectroscopic accuracy. The excited-state rovibrational levels are obtained

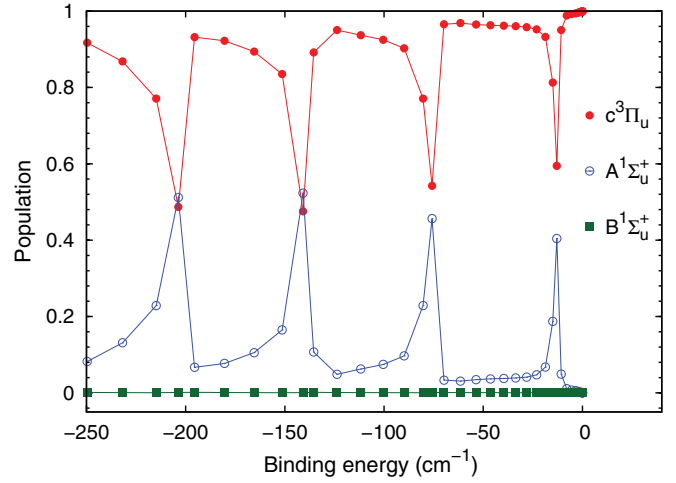


FIG. 3. (Color online) Population of the  $c^3\Pi_u$ ,  $A^1\Sigma_u^+$  and  $B^1\Sigma_u^+$  components of the  $0_u^+$  rovibrational levels for  $J' = 1$ . The binding energies are taken with respect to the  $\text{Sr}(^3P_1) + \text{Sr}(^1S)$  asymptote.

from diagonalization of the Hamiltonian (2) with  $E_0 = 0$ . Their analysis reveals a significant singlet-triplet mixing, cf. Fig. 3 presenting the  $c^3\Pi_u$ ,  $A^1\Sigma_u^+$ , and  $B^1\Sigma_u^+$  diabatic components of the coupled wave functions. This mixing results from the crossing between the  $c^3\Pi_u$  and  $A^1\Sigma_u^+$  states, which are coupled by spin-orbit interaction. On average, the rovibrational levels are predominantly of triplet character as expected for the  $^1S + ^3P$  asymptote. However, a sequence of peaks indicates the occurrence of rovibrational levels with very strong singlet-triplet mixing. These levels are particularly useful for both photoassociation and a subsequent bound-to-bound transition. This is illustrated in Fig. 4 showing the vibrational wave functions that correspond to the two rightmost peaks in the  $A^1\Sigma_u^+$ -state components of Fig. 3 (at binding energies of 12.9 and 75.8  $\text{cm}^{-1}$ ) and comparing them to the  $v' = -6$  wave func-

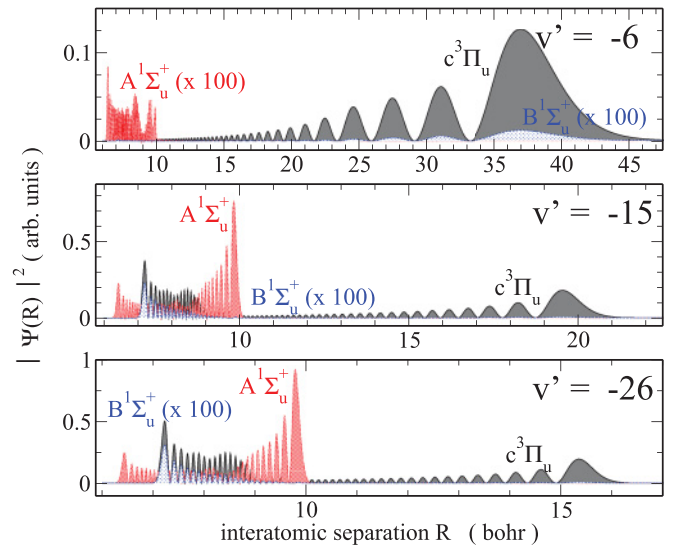


FIG. 4. (Color online) Vibrational wave functions of the coupled  $c^3\Pi_u$ ,  $A^1\Sigma_u^+$ , and  $B^1\Sigma_u^+$  electronic states for  $v' = -6$ ,  $v' = -15$ , and  $v' = -26$ . The corresponding binding energies are  $E_{v'=-6} = 0.27 \text{ cm}^{-1} = 8.09 \text{ GHz}$ ,  $E_{v'=-15} = 12.9 \text{ cm}^{-1}$ , and  $E_{v'=-26} = 75.8 \text{ cm}^{-1}$ . Note the different scale for the interatomic separation.

tion, the lowest level previously observed experimentally [17]. The  $v' = -6$  wave function is almost purely long-range and of predominantly triplet character, with the population of both singlet components being three orders of magnitude smaller than the triplet one (note that the wave functions of both the  $A^1\Sigma_u^+$  and  $B^1\Sigma_u^+$  components were scaled up by a factor of 100 to be visible in the figure). The picture changes completely for the levels  $v' = -15$  and  $v' = -26$ . Since the relative weights of the  $c^3\Pi_u$  and  $A^1\Sigma_u^+$  components are almost equal (cf. Fig. 3), the  $v' = -15$  and  $v' = -26$  wave functions in Fig. 4 display  $A^1\Sigma_u^+$  and  $c^3\Pi_u$  components on the same scale. Remarkably, the triplet wave functions also show peaks at short internuclear distance. This is a clear signature of resonant, nonadiabatic coupling between vibrational levels of the spin-orbit-coupled electronic states [14,33,34]. It occurs when two potential energy curves that are coupled cross and the energies of the two corresponding vibrational ladders coincide [33]. Then the vibrational wave functions reflect the turning points of the two potentials, as seen in Fig. 4. Resonant coupling was shown to lead to significantly enlarged bound-to-bound transition rates to form deeply bound molecules in their electronic ground state [14,35,36]. According to Fig. 4, it is the coupling between the  $c^3\Pi_u$  state and the  $A^1\Sigma_u^+$  state that becomes resonant, inducing strong mixing between these components. The effect of this resonant coupling will be further increased by the presence of the  $B^1\Sigma_u^+$  state in addition to the  $A^1\Sigma_u^+$  state. The behavior of the  $B^1\Sigma_u^+$  component strictly follows the  $c^3\Pi_u$  wave function, but is two orders of magnitude smaller (cf. Fig. 4). This is easily rationalized in terms of the  $B^1\Sigma_u^+$  component representing only a small admixture, due to the spin-orbit coupling  $\xi_2(R)$  in the Hamiltonian (2), to the principal part of the  $(1)0_u^+$  state that originates from the  $c^3\Pi_u$  potential. The magnitude of the  $B^1\Sigma_u^+$  component is straightforwardly estimated by treating the spin-orbit coupling as a perturbation and calculating the first-order correction to the wave function, similarly to the expression for the transition dipole moment, Eq. (1).

In the alkali-metal dimers, the spin-orbit coupling mixes in a triplet component that does not directly participate in the optical transition between singlet states [14,35,36]. Therefore, the enhancement of the bound-to-bound transitions in the alkali-metal dimers is only due to the modification of the singlet wave function. Here, for bound-to-bound transitions to the electronic ground state, the effective dipole is mainly due to the coupling between the  $c^3\Pi_u$  and the  $A^1\Sigma_u^+$  states [cf. Eq. (1)]. Therefore, it is not only the modification of the  $c^3\Pi_u$  wave function but also the presence of a large  $A^1\Sigma_u^+$  component that is responsible for the enhancement of bound-to-bound transitions. Both effects together, the additional peaks in the  $c^3\Pi_u$  wave function at interatomic separations  $R < 10$  bohr, and the large  $A^1\Sigma_u^+$  component at these interatomic separations lead to a significantly enhanced effective dipole moment according to Eq. (1). We thus find that for alkaline-earth-metal atoms near the  $^1S + ^3P_1$  intercombination line, the resonant coupling enlarges the singlet admixture to a predominantly triplet wave function and enhances both the bound-to-bound and the free-to-bound transition matrix elements. The enhancement of the bound-to-bound transitions significantly reduces the lifetime of the excited-state bound levels. The lifetimes of the levels  $v' = -15$  and  $v' = -26$  are found to be 30.9 and 27.2 ns,

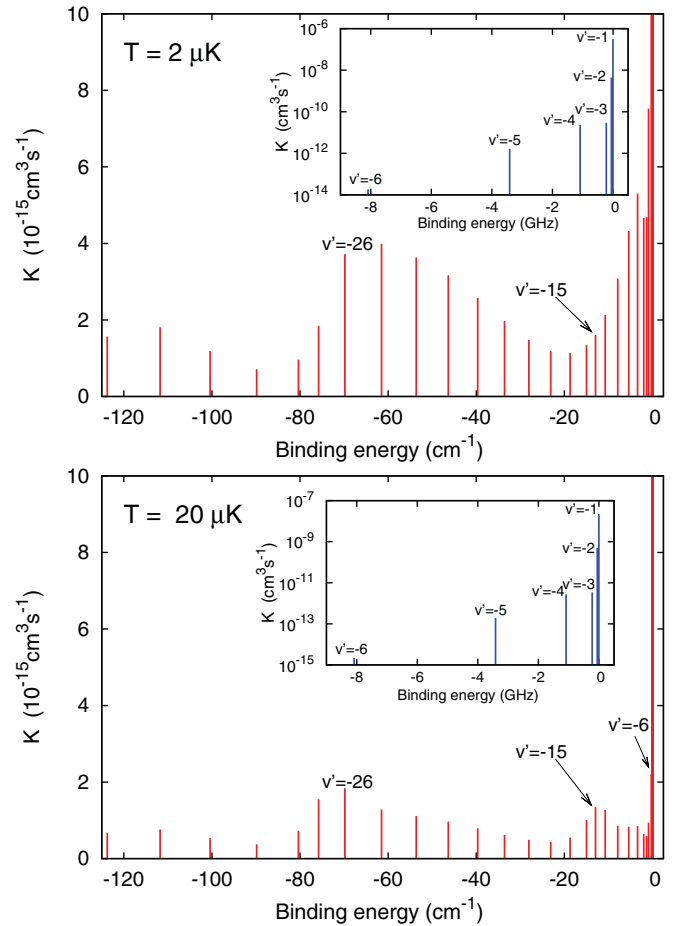


FIG. 5. (Color online) Photoassociation into rovibrational levels of the coupled  $c^3\Pi_u$ ,  $A^1\Sigma_u^+$ , and  $B^1\Sigma_u^+$  states below the  $\text{Sr}(^3P_1) + \text{Sr}(^1S)$  dissociation limit for a laser intensity  $I = 1 \text{ W/cm}^2$  and two temperatures,  $2 \mu\text{K}$  (upper panel) and  $20 \mu\text{K}$  (lower panel). The transitions to the six least-bound levels that were reported in Ref. [17] are shown in a semilogarithmic plot in the insert (note the different scales).

respectively, compared to  $7.61 \mu\text{s}$  for  $v' = -6$ , i.e., they are decreased by two orders of magnitude. This is rationalized by a larger spontaneous emission rate resulting from an enhancement in the bound-to-bound transitions according to Eq. (10).

The two effects, i.e., an increase in the bound-to-bound and free-to-bound transition matrix elements, have an opposite impact on the photoassociation probability, with the former hindering and the latter facilitating the photoassociation process. The photoassociation absorption coefficient [cf. Eq. (7)] is shown in Fig. 5 for all bound levels below the  $^1S + ^3P_1$  dissociation limit for two temperatures,  $T = 2 \mu\text{K}$  [29] and  $T = 20 \mu\text{K}$  [17]. The absorption coefficient for the levels that were experimentally observed [17] are shown in the inset of Fig. 5 using a logarithmic scale. At  $T = 2 \mu\text{K}$ , the peak rate coefficients for the strongly mixed levels  $v' = -15$  and  $v' = -26$  amount to  $K = 1.6 \times 10^{-15} \text{ cm}^3 \text{ s}^{-1}$  and  $K = 1.8 \times 10^{-15} \text{ cm}^3 \text{ s}^{-1}$ , respectively, compared to  $K = 1.9 \times 10^{-14} \text{ cm}^3 \text{ s}^{-1}$  for the lowest previously observed level,  $v' = -6$ , i.e., about one order of magnitude smaller. However, at  $T = 20 \mu\text{K}$  and also at higher temperatures, the levels with

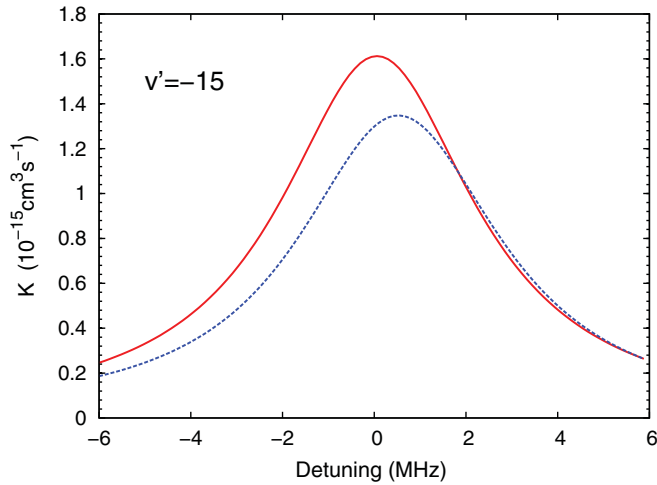


FIG. 6. (Color online) Shape of the photoassociation line for transition into the rovibrational level  $|v' = -15, J' = 1\rangle$  as a function of the detuning,  $\Delta_{v'J'}$ , from this level ( $I = 1 \text{ W/cm}^2$ ) at  $T = 2 \mu\text{K}$  (solid red line) and  $T = 20 \mu\text{K}$  (dashed blue line).

strong resonant coupling have absorption coefficients that are very similar to that of  $v' = -6$ ,  $K = 1.3 \times 10^{-15} \text{ cm}^3 \text{ s}^{-1}$ , and  $K = 1.6 \times 10^{-15} \text{ cm}^3 \text{ s}^{-1}$  for  $v' = -15$  and  $v' = -26$ , respectively, compared to  $K = 2.2 \times 10^{-15} \text{ cm}^3 \text{ s}^{-1}$  for  $v' = -6$  [see also bottom panel of Fig. 5]. The peak rate coefficients for the strongly mixed levels are less affected by temperature broadening. This is rationalized in terms of their large natural width, of the order of a few MHz. In contrast, for the level  $v' = -6$  the natural width amounts to merely 20 kHz. The natural widths need to be compared to thermal widths of 42 kHz and 0.42 MHz for  $T = 2 \mu\text{K}$  and  $T = 20 \mu\text{K}$ , respectively. For the strongly mixed levels, the photoassociation line shapes, shown in Fig. 6 for  $|v' = -15, J' = 1\rangle$ , are thus governed by the natural width, about 4.5 MHz in Fig. 6, and thermal broadening is of secondary importance even at a temperature of  $T = 20 \mu\text{K}$ . Due to the relatively short lifetime of the level, the profile manifests also only a very weak asymmetry.<sup>1</sup> For regular levels such as  $v' = -6$  the opposite holds, i.e., the thermal width is larger than the natural width. An increase in temperature from 2 to 20  $\mu\text{K}$  therefore has a noticeable effect on the photoassociation rate (cf. Ref. [37] for a detailed analysis of the effect of thermal broadening on the peak rate coefficients). We conclude that photoassociation of strontium atoms into strongly perturbed levels, albeit challenging, is within reach for an experimental setup such as that of Ref. [17].

After observing that photoassociation into resonantly perturbed levels such as  $v' = -15$  or  $v' = -26$  should be feasible experimentally, the transition moments from these levels into bound levels of the electronic ground state are examined in Fig. 7. Furthermore, Fig. 8 shows the modulus squared of the vibrationally averaged transition moments governing the spontaneous emission coefficients [cf. Eq. (10)] and the branching ratios [cf. Eq. (14)]. While the level  $v' = -6$

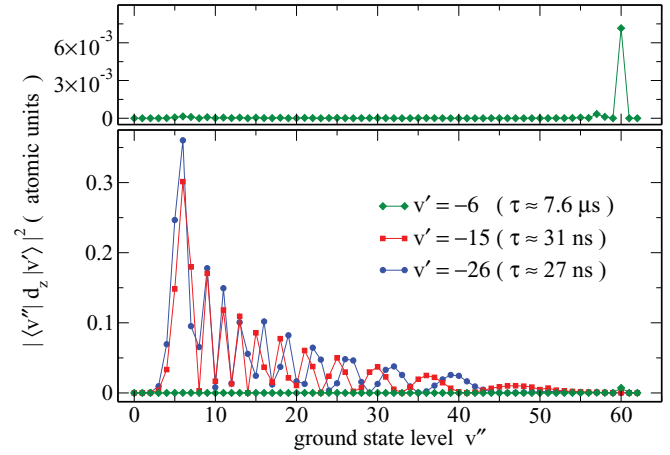


FIG. 7. (Color online) Modulus squared of the vibrationally averaged bound-to-bound electric transition dipole moments between excited-state rovibrational levels  $v' = -6$ ,  $v' = -15$ , and  $v' = -26$ , all with  $J' = 1$  (shown in Fig. 4) and all vibrational levels  $|v'', J'' = 0\rangle$  of the ground electronic state,  $X^1\Sigma_g^+$ .  $\tau$  denotes the lifetime for spontaneous decay to the  $X^1\Sigma_g^+$  state.

decays predominantly, with a branching ratio of more than 80%, into  $v'' = -3$ , a very weakly bound ground-state level with a binding energy of  $0.17 \text{ cm}^{-1}$ , the strongly perturbed levels  $v' = -15$  or  $v' = -26$  decay into a range of the ground-state levels, including deeply bound ones. The largest transition moment is observed for the ground-state level  $v'' = 6$  with a binding energy of  $836.4 \text{ cm}^{-1}$ . The corresponding branching ratios amount to about 17% for both  $v' = -15$  and  $v' = -26$ , compared to less than 2% for  $v' = -6$ . Note that the branching ratios to  $v'' = 6$  in Fig. 8 are almost equal for  $v' = -15$  and  $v' = -26$ , while the transition moments in Fig. 7 are not. This is due to the dependence of the spontaneous emission coefficients on the transition frequency in addition to the transition moment [cf. Eq. (10)]. Based on the favorable transition moments between the strongly perturbed excited-state levels and  $v'' = 6$ , stimulated emission using a

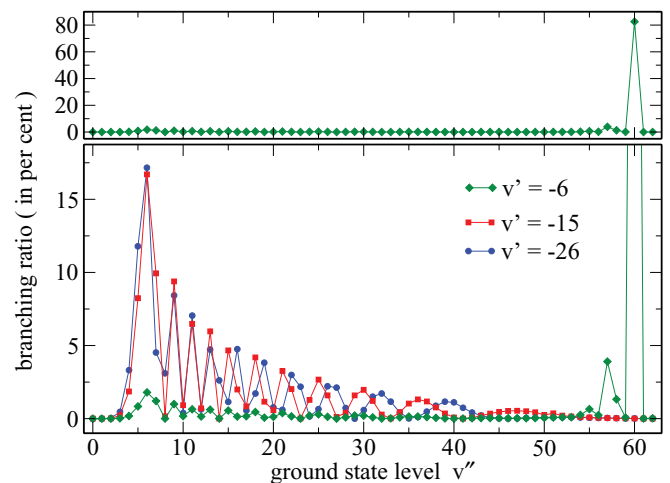


FIG. 8. (Color online) Branching ratio for the spontaneous decay from levels  $v' = -6$ ,  $v' = -15$ , and  $v' = -26$  to bound rovibrational levels of the ground electronic state.

<sup>1</sup>Note that the detuning in Fig. 6 is taken with respect to the binding energy  $E_{v'=-15, J'=1} = 12.9 \text{ cm}^{-1}$ , not with respect to the atomic transition frequency.

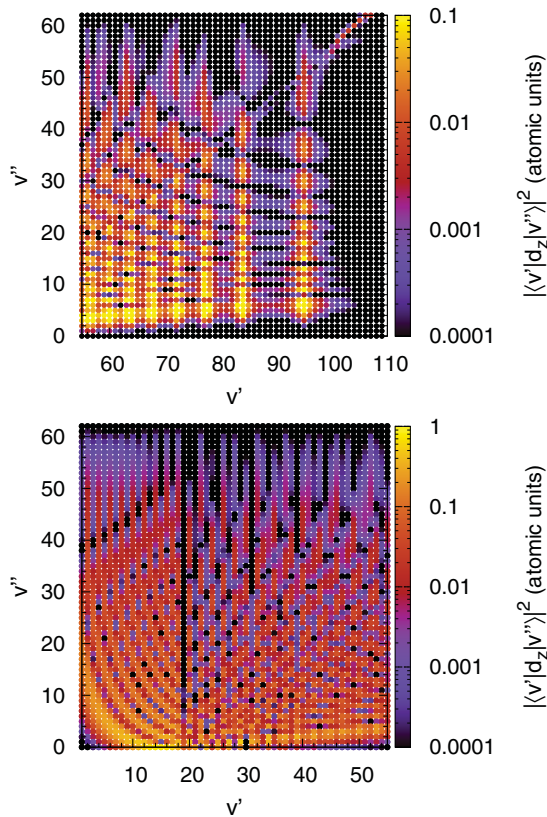


FIG. 9. (Color online) Modulus squared of the vibrationally averaged bound-to-bound electric transition dipole moments between all rovibrational levels  $|v', J' = 1\rangle$  of the  $0_u^+$  potential and all vibrational levels  $|v'', J'' = 0\rangle$  of the ground electronic state,  $X^1\Sigma_g^+$  (for other possible combinations of  $J'$  and  $J''$  the pattern is almost identical).

nanosecond pulse could be employed in order to pump the excited-state population selectively into the ground-state level  $v'' = 6$ . Alternatively, final state selectivity could be achieved by photoassociation via stimulated Raman adiabatic passage (STIRAP) [38]. It requires a sufficiently steep trap to ensure a well-defined phase of the initial state  $|E, J'\rangle$ , which is expected to be feasible in a deep optical lattice [39]. Due to their large transition moments for both pump and Stokes steps, the pathways  $E \rightarrow v' = -15(-26) \rightarrow v'' = 6$  would be the most promising routes for STIRAP photoassociation from an optical lattice into deeply bound levels.

A complete overview over transitions between the rovibrational levels  $v'$  of the excited  $0_u^+$  states below the  $^1S + ^3P_1$  asymptote and all ground-state levels  $v''$  is given by Fig. 9. For clarity, the figure has been separated into two parts, showing the highly excited state levels  $v'$  in the top panel and the lower excited state levels  $v'$  in the bottom panel of Fig. 9. Note that we find 110 excited state  $0_u^+$  levels  $v'$  below the  $^1S + ^3P_1$  asymptote with  $J' = 1$ , i.e.,  $v' = -6$  corresponds to  $v' = 104$ ,  $v' = -15$  to 95, and  $v' = -26$  to 84. Considering first levels close to the  $^1S + ^3P_1$  dissociation limit, we notice that the last two excited-state levels have extremely weak bound-to-bound transition moments. The next ten lower levels display a single peak in their transition moments, indicating pure Franck-Condon transitions close

to the outer turning point. This is typical for weakly bound, regular levels. Transferring the molecular population to shorter bond lengths is extremely difficult for such levels and requires many excitation-deexcitation cycles [38].

The first strongly perturbed level,  $v' = -15$  (or  $v' = 95$ ), leads to a prominent series of peaks in the squared transition moment matrix. Figure 9 indicates that also the neighboring levels of  $v' = -15$  are significantly perturbed. This would be important for pump-dump schemes using picosecond laser pulses [40,41]. An excited-state wave packet ideally suited for selective population transfer into  $v'' = -6$  is obtained by superimposing levels  $v' = 92, \dots, 98$ . This translates into a spectral width of the photoassociation pulse of  $15 \text{ cm}^{-1}$ , corresponding to a transform-limited pulse duration of 1 ps. Note that a previous study considering only the experimentally observed weakly bound levels concluded that short-pulse pump-dump photoassociation near the intercombination line transition is not viable [19]. The main obstacle is the quasi- $R^{-6}$  behavior of the excited-state potential that leads to a reduced density of vibrational levels for very small photoassociation detunings. The number of vibrational levels present is then too small to obtain a truly nonstationary wave packet [19]. However, the picture changes completely for more deeply bound excited-state levels such as those around  $v' = 95$ . The spectral width of the pulse can easily be chosen such that several vibrational levels are within the photoassociation window, without exciting the atomic intercombination line transition that would lead to loss of atoms [41]. The advantage of a time-dependent photoassociation scheme in the presence of nonresonant coupling lies in the dynamical interplay that arises between the interaction of the molecule with the laser light and the spin-orbit interaction. In such a situation, a dynamical enhancement of the final state population was found for strong dump pulses, indicating that the efficiency of population transfer is not determined by the transition matrix elements anymore [41].

A key question is how accurate our predictions are regarding the position of the perturbed levels such as  $v' = -15$  or  $v' = -26$ . There is no doubt about the presence of such levels since it results from the crossing between the  $c^3\Pi_u$  and  $A^1\Sigma_u^+$  potential energy curves, and this crossing was confirmed by a recent experimental study [25]. Our *ab initio* data reported in Ref. [21] are able to reproduce the rovibrational energy levels for  $J' = 1$  obtained from the fit of the experimental data to a Dunham-type expansion [25] to within  $0.64 \text{ cm}^{-1}$ . Considering all experimentally observed levels with  $J' \leq 50$ , the root-mean-square deviation between theoretically calculated levels and the raw experimental data is  $4.5 \text{ cm}^{-1}$ . Perhaps this value,  $\pm 4.5 \text{ cm}^{-1}$ , should be considered as a very conservative estimate of the error bars in the binding energies reported in the present study. The main sources of error in the binding energies are the inaccuracy of the  $c^3\Pi_u$  potential and its spin-orbit correction,  $A(R)$ . Scaling of the  $c^3\Pi_u$  potential or the  $A(R)$  coupling by  $\pm 5\%$  leads to shifts in the binding energies by  $2\text{--}2.5 \text{ cm}^{-1}$ , in particular, for the levels with strong singlet-triplet mixing. However, very good results for the  $A^1\Sigma_u^+$  state and for the atomic spin-orbit splitting of the  $^3P$  and  $^3D$  multiplets, obtained in Ref. [21], suggest the accuracy of the  $c^3\Pi_u$  potential and the  $A(R)$  coupling to be better than 5%. Note that scaling the other spin-orbit

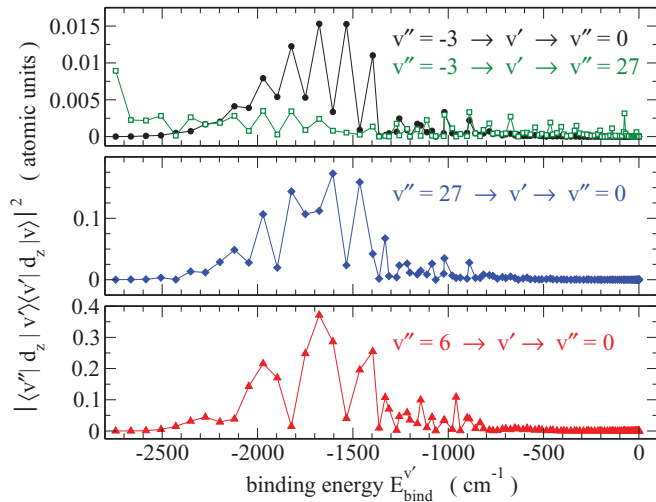


FIG. 10. (Color online) Vibrationally averaged bound-bound Raman transition moments as a function of the binding energy of the intermediate  $0_u^+$  rovibrational levels for three different pathways discussed in proposals for the measurement of the time variation of the electron-to-proton mass ratio,  $m_e/m_p$  [10,11]. Note the different scales for the transition moments.

couplings,  $\xi_1(R)$  and  $\xi_2(R)$ , by  $\pm 5\%$  has a negligible effect on the position of the bound levels. This confirms our assessment of the estimated error bars of  $\pm 4.5 \text{ cm}^{-1}$  as rather conservative. While such error bars might appear to be relatively large from an experimental perspective, they are not surprising for a system with 78 electrons, strong relativistic effects, and the  $A^1\Sigma_u^+$  potential as deep as  $8433 \text{ cm}^{-1}$  that are found in the strontium dimer.

The Franck-Condon parabola typical for transitions between regular vibrational levels [42,43] is absent in Fig. 9. This reflects the strong perturbation of the vibrational spectrum of the excited-state levels due to the spin-orbit interaction. A reasoning on possible optical pathways solely based on the shape of the adiabatic potentials will therefore give a wrong picture. To emphasize this point, Fig. 10 presents the transition matrix elements for Raman transitions that are relevant in the proposal for the measurement of the time variation of the electron-to-proton mass ratio,  $m_e/m_p$  [10,11]. The idea is to transfer molecules into the  $X^1\Sigma_g^+$  ground vibrational level starting from the weakly bound ground-state level  $v'' = -3$  (corresponding to  $v'' = 60$ ) that is populated by spontaneous decay from  $v' = -6$ , the lowest excited-state level previously observed in a photoassociation experiment [17]. One could expect the efficiency of a direct transfer  $v'' = -3 \rightarrow v' \rightarrow v'' = 0$  to be much smaller than the efficiency of a two-Raman-step transfer employing an intermediate state,  $v'' = 27$ . Inspection of Fig. 10 reveals, however, that this expectation is not confirmed. There exist a few excited-state levels, with binding energies between  $2000$  and  $1400 \text{ cm}^{-1}$ , that have large transition dipole moments with both  $v'' = -3$  (or  $v'' = 60$ ) and  $v'' = 0$ , yielding a high efficiency for Raman transfer directly from  $v'' = -3$  to  $v'' = 0$ . The maximum Raman moments are found for  $v' = 14$  and  $v' = 16$  [cf. Fig. 9]. These levels are almost pure singlet rovibrational states belonging to the  $A^1\Sigma_u^+$  potential, and are only marginally perturbed by the

spin-orbit coupling. For all the pathways presented in Fig. 10 the most favorable intermediate levels  $v'$  are those which are energetically the highest and yet almost unperturbed, i.e., the levels located just below the crossing between the  $c^3\Pi_u$  and  $A^1\Sigma_u^+$  potential-energy curves. This is easily rationalized in terms of the strong transition dipole moment,  $d_z(A \leftarrow X)$ , of these levels and their relatively good overlap with the rovibrational levels of the  $X^1\Sigma_g^+$  potential. The decrease of the Raman transition moments for the deeply bound levels excited-state levels, with  $v' \leq 10$  and binding energies larger than  $2000 \text{ cm}^{-1}$ , is due to shift of equilibrium positions of the  $A^1\Sigma_u^+$  and  $X^1\Sigma_g^+$  potential wells [cf. Fig. 1].

The Raman transition moments from  $v'' = -3 \rightarrow v' = 14/16 \rightarrow v'' = 0$  are larger than any of the moments for transfer from  $v'' = -3$  to  $v'' = 27$ . Of course, even higher Raman transition moments are found for optical pathways to  $v'' = 0$  that start in  $v'' = 6$  (cf. bottom panel of Fig. 10), the level that is populated by photoassociation into a strongly perturbed excited-state level followed by spontaneous or stimulated emission or pump-dump photoassociation, as explained above. We thus conclude that a single Raman transition after photoassociation is sufficient to obtain molecules in the  $X^1\Sigma_g^+$  ground vibrational level. The least intensity of the Raman lasers is required for optical pathways starting from  $v'' = 6$ , i.e., after photoassociation into strongly perturbed levels such as  $v' = -15$  or  $v' = -26$ . The pathways starting from  $v'' = 6$  come with the additional advantage that the transition frequencies of the Raman lasers differ only by  $E_{v''=0} - E_{v''=6} \approx 225 \text{ cm}^{-1}$  compared to  $792 \text{ cm}^{-1}$  for  $v'' = 27 \rightarrow v'' = 0$  or  $1061 \text{ cm}^{-1}$  for  $v'' = -3 \rightarrow v'' = 0$ . We would like to stress here that all these conclusions concerning the Raman transitions should strictly be valid as the intermediate  $v'$  levels between  $2000$  and  $1400 \text{ cm}^{-1}$  are located in the bottom of the  $A^1\Sigma_u^+$  well where the potential is known precisely [21,25], and are almost not perturbed by the spin-orbit interaction. This also means that doing high-precision Raman spectroscopy with these states should be feasible and the spectra will not be obscured by the spin-orbit perturbation effects.

#### IV. SUMMARY AND CONCLUSIONS

Based on state-of-the-art *ab initio* calculations, we have calculated photoassociation rates and spontaneous emission coefficients for the photoassociation of  $\text{Sr}_2$  molecules near the  $^1S + ^3P_1$  intercombination line transition. We have also analyzed bound-to-bound transition moments as well as Raman transition moments connecting vibrational levels in the electronic ground state, relevant to achieve transfer into the  $X^1\Sigma_g^+$  ground vibrational level. The vibrational spectrum of the coupled  $c^3\Pi_u$ ,  $A^1\Sigma_u^+$ ,  $B^1\Sigma_u^+$  excited-state manifold is found to be strongly perturbed. Therefore, optical pathways cannot be predicted based on the turning points of the adiabatic potentials. Consequently, the theoretical analysis needs to fully account for the spin-orbit coupling of the electronically excited states.

For excited-state binding energies of about  $13 \text{ cm}^{-1}$  and larger, up to  $2000 \text{ cm}^{-1}$ , strongly perturbed vibrational levels are identified. The strong perturbations result from the resonant interaction of the coupled vibrational ladders of the  $c^3\Pi_u$  and  $A^1\Sigma_u^+$  states. For  $\text{Sr}_2$ , these levels are found to be particularly

well suited for the stabilization of photoassociated molecules to the electronic ground state, either via spontaneous or stimulated emission. The photoassociation rate of the strongly perturbed levels is calculated to be comparable to that of the lowest level previously observed [17] at a temperature of  $T = 20 \mu\text{K}$  and about one order of magnitude smaller at  $T = 2 \mu\text{K}$ . We therefore conclude that photoassociation into strongly perturbed levels should be feasible with the currently available experimental techniques.

Strongly perturbed levels display large bound-to-bound transition moments with deeply bound vibrational levels of the electronic ground state. If photoassociation is followed by spontaneous emission, this will show up as a dominant decay into  $X^1\Sigma_g^+(v'' = 6)$ , although a large range of ground-state vibrational levels will be populated as well. State selectivity of the ground-state levels can be achieved by stimulated emission, either employing STIRAP photoassociation in a deep optical lattice [39] or pump-dump photoassociation with picosecond pulses [40,41].

Identifying in the experiment the strongly perturbed levels of the  $c^3\Pi_u, A^1\Sigma_u^+, B^1\Sigma_u^+$  manifold that are particularly suitable for efficient stabilization to deeply bound ground-state levels requires a spectroscopic search since even state-of-the-art *ab initio* methods cannot predict the positions of the rovibrational levels with precision better than a few wave numbers for such a heavy system like Sr<sub>2</sub>. The theoretical precision is limited here mainly by uncertainty of the  $c^3\Pi_u$  state and its relativistic correction, and can be reduced only after emergence of new experimental data concerning the  $c^3\Pi_u, A^1\Sigma_u^+, B^1\Sigma_u^+$  manifold of Sr<sub>2</sub>.

Finally, the crossing between  $A^1\Sigma_u^+$  and  $c^3\Pi_u$  potentials will be important not only for the initial formation of Sr<sub>2</sub>

molecules but also for any subsequent Raman-type transition proceeding via the coupled  $c^3\Pi_u, A^1\Sigma_u^+, B^1\Sigma_u^+$  manifold of states. The presence of unperturbed levels of the  $A^1\Sigma_u^+$  state, that are located just below the crossing with the  $c^3\Pi_u$  curve, leads to the somewhat unexpected result that the weakly bound  $X^1\Sigma_g^+$  vibrational levels just below the dissociation limit show larger Raman transition moments with the ground vibrational level than with levels half-way down the ground-state potential well. Direct Raman transitions to the ground vibrational level thus become possible for both weakly and strongly bound levels. When utilizing these transitions for population transfer by STIRAP, deeply bound levels such as  $v'' = 6$  come with the advantage of a smaller frequency gap between the pump and Stokes pulse and significantly larger transition moments translating into lower pulse amplitudes.

There are thus at least two good reasons for future experiments on the strontium dimer to employ strongly perturbed levels of the  $c^3\Pi_u, A^1\Sigma_u^+, B^1\Sigma_u^+$  manifold: efficient stabilization to deeply bound ground-state levels and large matrix elements for Raman transitions between ground-state levels. Our calculations show these experiments to be feasible with currently available experimental technology.

#### ACKNOWLEDGMENTS

We would like to thank Tanya Zelevinsky, Paul Julienne, and Svetlana Kotochigova for many useful discussions. This study was supported by the Polish Ministry of Science and Higher Education through the project N N204 215539. Financial support from the Deutsche Forschungsgemeinschaft (Grant No. KO 2301/2) is also gratefully acknowledged.

- 
- [1] A. D. Ludlow, T. Zelevinsky, G. K. Campbell, S. Blatt, M. M. Boyd, M. H. G. de Miranda, M. J. Martin, J. W. Thomsen, S. M. Foreman, J. Ye *et al.*, *Science* **319**, 1805 (2008).
- [2] M. Takamoto, F.-L. Hong, R. Higashi, and H. Katori, *Nature (London)* **435**, 321 (2005).
- [3] M. D. Swallows, M. Bishof, Y. Lin, S. Blatt, M. J. Martin, A. M. Rey, and J. Ye, *Science* **331**, 1043 (2011).
- [4] S. Falke, H. Schnatz, J. S. R. V. Winfred, T. Middelmann, S. Vogt, S. Weyers, B. Lipphardt, G. Grosche, F. Riehle, U. Sterr *et al.*, *Metrologia* **48**, 399 (2011).
- [5] A. Yamaguchi, N. Shiga, S. Nagano, Y. Li, H. Ishijima, H. Hachisu, M. Kumagai, and T. Ido, *Appl. Phys. Express* **5**, 022701 (2012).
- [6] P. G. Westergaard, J. Lodewyck, L. Lorini, A. Lecallier, E. A. Burt, M. Zawada, J. Millo, and P. Lemonde, *Phys. Rev. Lett.* **106**, 210801 (2011).
- [7] M. Chalony, A. Kastberg, B. Klappauf, and D. Wilkowski, *Phys. Rev. Lett.* **107**, 243002 (2011).
- [8] R. Ciuryło, E. Tiesinga, and P. S. Julienne, *Phys. Rev. A* **71**, 030701 (2005).
- [9] S. Blatt, T. L. Nicholson, B. J. Bloom, J. R. Williams, J. W. Thomsen, P. S. Julienne, and J. Ye, *Phys. Rev. Lett.* **107**, 073202 (2011).
- [10] T. Zelevinsky, S. Kotochigova, and J. Ye, *Phys. Rev. Lett.* **100**, 043201 (2008).
- [11] S. Kotochigova, T. Zelevinsky, and J. Ye, *Phys. Rev. A* **79**, 012504 (2009).
- [12] K. M. Jones, E. Tiesinga, P. D. Lett, and P. S. Julienne, *Rev. Mod. Phys.* **78**, 483 (2006).
- [13] A. Fioretti, D. Comparat, A. Crubellier, O. Dulieu, F. Masnou-Seeuws, and P. Pillet, *Phys. Rev. Lett.* **80**, 4402 (1998).
- [14] C. M. Dion, C. Drag, O. Dulieu, B. Laburthe Tolra, F. Masnou-Seeuws, and P. Pillet, *Phys. Rev. Lett.* **86**, 2253 (2001).
- [15] S. B. Nagel, P. G. Mickelson, A. D. Saenz, Y. N. Martinez, Y. C. Chen, T. C. Killian, P. Pellegrini, and R. Côté, *Phys. Rev. Lett.* **94**, 083004 (2005).
- [16] P. G. Mickelson, Y. N. Martinez, A. D. Saenz, S. B. Nagel, Y. C. Chen, T. C. Killian, P. Pellegrini, and R. Côté, *Phys. Rev. Lett.* **95**, 223002 (2005).
- [17] T. Zelevinsky, M. M. Boyd, A. D. Ludlow, T. Ido, J. Ye, R. Ciuryło, P. Naidon, and P. S. Julienne, *Phys. Rev. Lett.* **96**, 203201 (2006).
- [18] Y. N. Martinez de Escobar, P. G. Mickelson, P. Pellegrini, S. B. Nagel, A. Traverso, M. Yan, R. Côté, and T. C. Killian, *Phys. Rev. A* **78**, 062708 (2008).
- [19] C. P. Koch, *Phys. Rev. A* **78**, 063411 (2008).

- [20] C. P. Koch and R. Moszyński, *Phys. Rev. A* **78**, 043417 (2008).
- [21] W. Skomorowski, F. Pawłowski, C. P. Koch, and R. Moszynski, e-print [arXiv:1203.4524](https://arxiv.org/abs/1203.4524).
- [22] H. A. Bethe and E. E. Salpeter, *Quantum Mechanics of One- and Two-Electron Atoms* (Academic Press, New York, 1957), p. 170.
- [23] B. Bussery-Honvault, J.-M. Launay, T. Korona, and R. Moszynski, *J. Chem. Phys.* **125**, 114315 (2006).
- [24] A. Stein, H. Knöckel, and E. Tiemann, *Phys. Rev. A* **78**, 042508 (2008).
- [25] A. Stein, H. Knöckel, and E. Tiemann, *Eur. Phys. J. D* **64**, 227 (2011).
- [26] R. Napolitano, J. Weiner, C. J. Williams, and P. S. Julienne, *Phys. Rev. Lett.* **73**, 1352 (1994).
- [27] K. Sando and A. Dalgarno, *Mol. Phys.* **20**, 103 (1971).
- [28] B. Bussery-Honvault, J.-M. Launay, and R. Moszynski, *Phys. Rev. A* **72**, 012702 (2005).
- [29] T. Zelevinsky, S. Blatt, M. M. Boyd, G. K. Campbell, A. D. Ludlow, and J. Ye, *Chem. Phys. Chem.* **9**, 375 (2008).
- [30] V. Kokoouline, O. Dulieu, R. Kosloff, and F. Masnou-Seeuws, *J. Chem. Phys.* **110**, 9865 (1999).
- [31] K. Willner, O. Dulieu, and F. Masnou-Seeuws, *J. Chem. Phys.* **120**, 548 (2004).
- [32] S. Kallush and R. Kosloff, *Chem. Phys. Lett.* **433**, 221 (2006).
- [33] C. Amiot, O. Dulieu, and J. Vergès, *Phys. Rev. Lett.* **83**, 2316 (1999).
- [34] S. Ghosal, R. J. Doyle, C. P. Koch, and J. M. Hutson, *New J. Phys.* **11**, 055011 (2009).
- [35] H. K. Pechkis, D. Wang, Y. Huang, E. E. Eyler, P. L. Gould, W. C. Stwalley, and C. P. Koch, *Phys. Rev. A* **76**, 022504 (2007).
- [36] A. Fioretti, O. Dulieu, and C. Gabbanini, *J. Phys. B* **40**, 3283 (2007).
- [37] R. Ciuryło, E. Tiesinga, S. Kotochigova, and P. S. Julienne, *Phys. Rev. A* **70**, 062710 (2004).
- [38] C. P. Koch and M. Shapiro, *Chem. Rev.* (2012).
- [39] M. Tomza, F. Pawłowski, M. Jeziorska, C. P. Koch, and R. Moszynski, *Phys. Chem. Chem. Phys.* **13**, 18893 (2011).
- [40] C. P. Koch, E. Luc-Koenig, and F. Masnou-Seeuws, *Phys. Rev. A* **73**, 033408 (2006).
- [41] C. P. Koch, R. Kosloff, and F. Masnou-Seeuws, *Phys. Rev. A* **73**, 043409 (2006).
- [42] M. Viteau, A. Chotia, M. Allegrini, N. Bouloufa, O. Dulieu, D. Comparat, and P. Pillet, *Science* **321**, 232 (2008).
- [43] M. Viteau, A. Chotia, D. Sofikitis, M. Allegrini, N. Bouloufa, O. Dulieu, D. Comparat, and P. Pillet, *Faraday Discuss.* **142**, 257 (2009).